(Preprint) AAS 09-227

THE ENDGAME PROBLEM PART B: THE MULTI-BODY TECHNIQUE AND THE T-P GRAPH

Stefano Campagnola * **and Ryan P. Russell** †

ESA and NASA renewed interest on missions to Europa, Ganymede and Titan poses the question on how to best solve the Endgame problem. Endgames typically aim at a cheap insertion maneuver into the science orbit, and can be designed using either Vinfinity Leveraging Maneuvers (VILMs) or the Multi-Body dynamics. Although historically linked to insertion maneuvers, the endgame problem is symmetric and equally applies to departure. In this paper series, we analyze and draw connections between the two apparently separate approaches, providing insight to the dynamics of multi-body gravity assist problem. In this paper we study the anatomy of the Multi-Body approach using a new graphical tool, the Tisserand-Poincaré (T-P) graph. The T-P graph shows that ballistic endgames are energetically possible and it explains why they require resonant orbits patched with high altitude flybys, whereas in the VILM approach flybys alone are not effective without impulsive maneuvers in between them. We then explain how to use the T-P graph and the associated concepts to design quasi-ballistic transfers composed by endgames and begingames (the symmetric problems). Unlike previous methods, the T-P graph provides a valuable, energy based, target point for the design of the two parts of the trajectory, and a simple way to patch them. Further, the patch point calculation is straight forward and does not require the often tedious generation of manifolds and their associated intersections. We finally present two transfers. The first transfer is between low-altitude orbits at Europa and Ganymede using almost half the Δv of the Hohmann transfer; the second transfer is a 300-day quasi-ballistic transfer between halo orbits of the Jupiter-Ganymede and Jupiter-Europa. With some 50 m/s the transfer can be reduced by two months. While the results have the most relevant implications at low energy (endgame) levels, the Tisserand integral shows that ballistic multi-body transfers are feasible (given infinite time) for all energy levels across any distance gap.

INTRODUCTION

In the recent years both NASA and ESA studied a variety of mission options to the Galilean moons at Jupiter and to the Saturn moons including Enceladus and Titan. A very challenging part of the trajectory design of these missions is the Endgame,[1] the last part of the transfer before the insertion maneuver into the science orbit. The Endgame aims at a low Δv orbit insertion maneuver. The 'Begingame' is the symmetric problem and starts with a low Δv escape from an initial orbit around a minor body. Both transfers have been studied, designed and implemented on space missions with two distinct approaches.

The first approach uses the $v_\infty-$ Leveraging Maneuver (VILM) technique, where the combined effect of gravity assists and impulsive maneuvers (at the almost opposite apsidal point of the spacecraft orbit) changes the spacecraft relative velocity to the minor body.[2,3] Typically the transfer is first computed in the linked-conics model (i.e. the zero radius sphere of influence, patched-conics model), and then optimized in a real ephemeris model and patched together to the rest of the trajectory. The VILM approach is very intuitive and quickly provides fast solutions.

The second approach uses the Multi-body Technique,[4,5] where small Δv's (if any) are applied when the spacecraft is far from the minor body, typically to target high altitude flyby passages which produce the most favorable effects (e.g. behind or in front of the minor body to increase or decrease the spacecraft energy). The trajectory is computed directly in the real ephemeris model, or in the restricted three, four or five body

*Ph.D. student, University of Southern California, Aerospace and Mechanical Engineering, 854 Downay Way RRB, Los Angeles, CA 90089-1191, stefano.campagnola@missionanalysis.org

†Assistant Professor, Georgia Institute of Technology, Guggenheim School of Aerospace Engineering, 270 Ferst Drive, Atlanta, GA 30332-0150, ryan.russell@gatech.edu.

problem. This approach cannot be explained with the linked-conics model, where ballistic transfers cannot change the arrival conditions at the minor body. Trajectories are typically found with some heuristic method. Recently, nonlinear dynamical system theory has been used to help the design of Endgames or MultiMoon orbiters.[6,7,8] Usually the Multi-body Technique results in low cost, long time of flight trajectories. The Smart1 mission successfully implemented this strategy to get the spacecraft gravitationally captured around the Moon.[5]

In the two papers The Endgame Problem Part A[9] and Part B we study the Endgame transfers in general, and show the connections between the two approaches. The second part of the work, presented in this paper, studies the anatomy of the Multi-body Technique.

In the first section we recall the linked-conic and the patched circular restricted 3 body problem (CR3BP) models, and show how to transform the linked-conic gravity assist parameter in a state vector to be used in the CR3BP. We then consider two VILM endgames at Europa which were presented in Part A and use them as first guesses for the design of endgames in the CR3BP. The results show that although some VILM solutions cost almost the same, their total Δv might differ of as much as 10% when computed in a more accurate model. In general, the VILM approach should be used for fast preliminary design only if lower-cost longer-transfer solutions are *not* an option. Quasi-ballistic endgames and transfers cannot be designed either using the VILM approach or starting from VILM solutions, hence the need for a more accurate model and design strategy.

In the second section we introduce a Poincaré section in the negative x-axis of the rotating reference frame of the CR3BP. Far from the minor body the spacecraft trajectory is very similar to a Keplerian orbit; thus we can compute the osculating orbital elements of the spacecraft as it crosses the section, and plot them in a pericenter vs apocenter graph. On the same graph we plot Tisserand parameter level sets: the Tisserand parameter T is an approximation of the Jacobi constant, and it is very accurate when far from the minor body and for small mass parameters. The result is the Tisserand-Poincaré (T-P) graph, which is a natural extension of the Tisserand graph, as the v_∞ level sets are synonymous to Tisserand level sets noting that $T = 3 - v_\infty^2$ (see appendix). Yet the Tisserand level sets extend beyond the v_∞curves well into the regions where v_∞ is not feasible in the linked-conic models ($v_\infty^2 < 0$ if $T > 3$). Therefore when considering the conservation of the Tisserand parameter, the T-P graph demonstrates that ballistic transfers between moons are energetically possible despite the contrary conclusion derived from linked-conics theory. This is the first important result of the T-P graph.

In the third section we analyze the T-P graph in more detail. We use it to explain the MultiMoon Orbiter[4] and to explain in general the anatomy of Multi-Body Techniques. We focus on ballistic endgames and question the need for multiple flybys and resonant orbits, noting that ballistic transfers do not change the Jacobi constant and hence do not change the arrival speed at the minor body (the *ballistic endgame paradox*). Then we use the T-P graph to solve the paradox, showing that at low energy levels, high altitude flybys of the minor body are the only ballistic mechanism to move along the Tisserand curves and to reach the target altitude at the minor body.

In the last section we design transfers between Europa end Ganymede. Using the considerations from the previous section, we find trajectories that move through the graph in the shortest time and reach a prespecified target point on the T-P graph, which is the intersection of the Tisserand level sets of the endgame at Europa and begingame at Ganymede. In particular we compute a transfer from a circular orbit at Ganymede to a circular orbit at Europa for comparison with the VILMs solutions. We also compute a transfer between a halo orbit at Ganymede and a halo orbit at Callisto; in both cases the T-P graph provides an estimate of Δv. We argue that, while the total cost might increase in the full ephemeris model due to the fourth body perturbations, non-circular orbits, and change of plane maneuvers. We also argue however that a robust optimization algorithm should reduce the conservatively estimated costs with the introduction of several small mid-course maneuvers.

ENDGAMES FROM LINKED-2BP TO CR3BP

The conventional method for designing endgame trajectories is by patching v_∞-leveraging maneuvers (VILMs) in the linked-conic model.[10,9,1] Yet near ballistic endgames have been designed only in more accurate models, like the restricted 5-body problem[4] or the full ephemeris model.[5] In this work, we use the circular restricted three-body problem (CR3BP) model to design ballistic endgames, and patched CR3BP models to design transfers between moons.

In this section we briefly recall the linked-conics and the (patched) CR3BP models, and we show how to reproduce a linked-conics gravity assist in the planar, CR3BP. We then consider two very similar Europa endgames in the linked-conics model (designed using the leveraging graphs[9]) and optimize them in the CR3BP model. The results give insight into the difference between the two models, and into the limitations of the lower fidelity VILM approach when designing long flight time, low-cost endgame trajectories.

Linked-conics and CR3BP model

The *linked-conics model* (or zero radius sphere of influence, patched-conics model) is often used in the design of multiple gravity assist trajectories. The spacecraft and the minor bodies move as point masses on Keplerian orbits around the major body. If the spacecraft reaches one of the minor bodies, a gravity assist takes place and is modeled as an instantaneous change in the direction of the relative velocity v_∞ by an angle*

$$\delta = 2 \arcsin \frac{\tilde{\mu}_M}{\tilde{\mu}_M + \tilde{r}_\pi \tilde{v}_\infty^2} \tag{1}$$

Here and in the rest of the paper the tilde indicates dimensional quantities; variables without the tilde have been normalized using the usual space, time, and mass scale factors:

$$l^* = \tilde{a}_M, \qquad t^* = \sqrt{\frac{\tilde{a}_M^3}{\tilde{\mu}_P + \tilde{\mu}_M}} \qquad m^* = \tilde{m}_M + \tilde{m}_P$$

Also, lower case letters refer to variables in the inertial reference frame while upper case letters refer to variables in the rotating reference frame.

In the CR3BP model the gravity of both the major body and the minor body affects the motion of the spacecraft at all times. The major and minor bodies move in circular motion around their barycenter, and the spacecraft is massless. The equations of motion for the spacecraft are usually expressed in the rotating adimensional reference frame:[11]

$$\begin{cases} \ddot{X} - 2\dot{Y} &= \frac{\partial \Omega}{\partial X} \\ \ddot{Y} + 2\dot{X} &= \frac{\partial \Omega}{\partial Y} \\ \ddot{Z} &= \frac{\partial \Omega}{\partial Z} \end{cases} \tag{2}$$

$$\Omega(X,Y,Z) \equiv \frac{1}{2}\left(X^2 + Y^2\right) + \frac{1-\mu}{R_1} + \frac{\mu}{R_2} + \frac{1}{2}(1-\mu)\,\mu \tag{3}$$

where $R_1 = \sqrt{(X+\mu)^2 + Y^2 + Z^2}$ and $R_2 = \sqrt{(X+\mu-1)^2 + Y^2 + Z^2}$ are the distances to the primaries, and $\mu = \mu_M = \frac{\tilde{m}_M}{\tilde{m}_M + \tilde{m}_P}$ is the mass parameter. It is well known[12,11] that the system of Eq. (2) has one integral of motion, the Jacobi constant:

$$J = 2\Omega - V^2 = \left(X^2 + Y^2\right) + 2\frac{1-\mu}{R_1} + 2\frac{\mu}{R_2} + (1-\mu)\,\mu - V^2 \tag{4}$$

where $V^2 = \left(\dot{X}^2 + \dot{Y}^2 + \dot{Z}^2\right)$ is the velocity in the rotating frame. The Jacobi constant is used to define regions of motion. The system of Eq. (2) also has five fixed points, the Lagrangian points $L_i, i = 1, \ldots, 5$.

*The notation is explained in the Notation section at the end of the paper.

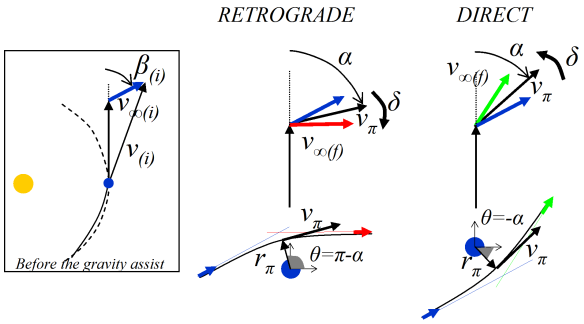

Figure 1. Direct and retrograde gravity assists.

In the rest of the paper, unless specified, we use the *planar* CR3BP , noting that the spacecraft trajectory is very close to the minor body orbital plane for the applications of interest here (i.e. missions to the Jupiter or Saturn moons).

In the design of transfers between moons, several minor bodies affect the spacecraft trajectory. In this case we use the *patched CR3BP model*, i.e. we split the trajectory in phases where only one minor body at a time affects the motion of the spacecraft around the major body. In each phase we use the corresponding minor body in the CR3BP model, and the boundary points of contiguous phases are patched together, sometimes using impulsive maneuvers.

Flyby models

In this section we reproduce a linked-conic gravity assist in the CR3BP. In particular we use the parameters of the linked-conic gravity assist to generate the vector state of the spacecraft at r_π, the closet approach to the minor body. We focus on the planar case, because we will use the results to reproduce VILMs in the CR3BP. Figure 1 shows the schematic of the direct and retrograde gravity assists.

From the velocity $v_{(i)}$ and flight path angle γ of the spacecraft just before the encounter we find

$$v_\infty = \sqrt{1 + v_{(i)}^2 - 2v_{(i)}\cos\gamma} \quad , \quad \beta_{(i)} = \arcsin\frac{v_{(i)}\cos\gamma}{v_\infty} \tag{5}$$

The gravity assist parameters r_π and σ ($\sigma = 1$ for direct gravity assists and $\sigma = -1$ for retrograde gravity assists) provide the deviation angle with Eq. (1), but also the norm and direction of the velocity at pericenter v_π, as shown in Figure 1 and in the following equations:

$$v_\pi = \sqrt{v_\infty^2 + 2\mu/r_\pi} \quad , \quad \alpha = \beta_{(i)} - \sigma\delta/2 \tag{6}$$

Now we can write the state s of the spacecraft at the closest approach in the inertial reference frame centered in the minor body. Always referring to figure 1, we find :

$$\theta = -\alpha + (\sigma - 1)\,\pi/2 \quad , \quad s = (r_\pi\cos\theta, r_\pi\sin\theta, -\sigma v_\pi\sin\theta, \sigma v_\pi\cos\theta) \tag{7}$$

Finally we apply the transformation of coordinate (see appendix A1) to find the state vector in the rotating reference frame:

$$S = ((1-\mu) + r_\pi\cos\theta, r_\pi\sin\theta, -(\sigma v_\pi - r_\pi)\sin\theta, (\sigma v_\pi - r_\pi)\cos\theta) \tag{8}$$

We now consider the special case $\beta_{(i)} = 0$ (the case when the v_∞ vector is aligned with the body velocity vector), which we use in the next section. From Eq. (6) and Eq. (7) we find

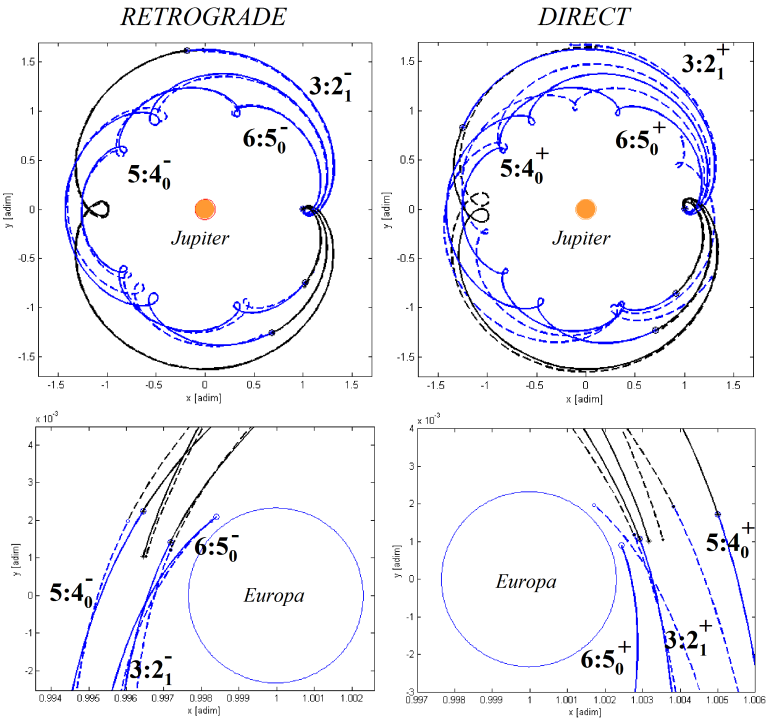

Figure 2 Long-transfer (direct) and short-transfer (retrograde) endgames at Europa optimized in the CR3BP (solid lines). Initially the VILM solutions are used to find the times of the midcourse and the states and times of the spacecraft at the close approaches. Those states are then propagated backward and forward in time in the CR3BP generating the first guess solutions (dash lines) for the optimization problem.

$$\theta = -\frac{\pi}{2} + \sigma\left(\frac{\pi}{2} + \delta\right) \tag{9}$$

Endgame optimization in the CR3BP

In this section we compute two endgames in the CR3BP. We take two VILM endgames at Europa presented in,[9] reproduce them in the CR3BP and use them as first guesses for an optimization algorithm which minimize the total Δv.

The first endgame is a sequence of long-transfer VILMs: $3:2_1^+, 4:3_0^+, 5:6_0^+$, where the plus sign refers to a long-transfer VILM. The second endgame is a sequence of short-transfer VILMs: $3:2_1^-, 4:3_0^-, 5:6_0^-$, where the minus sign in refers to a short-transfer VILM. Both endgames require some 150m/s to decrease the v_∞ from 1.8 km/s to approx. 0.8 km/s, and both endgames are composed by VILMs in which $\beta_{(i)} = 0$. However the long-transfer VILMs are linked by direct gravity assists ($\sigma = 1$) while the short transfer VILMs are linked by retrograde gravity assists ($\sigma = -1$).

As a consequence, Eq. (9) shows that the closest approaches of the first endgame occur on the L2 side ($-\pi/2 < \theta < \pi/2$), while the closest approaches of the second endgame occur on the L1 side ($\pi/2 < \theta < 3\pi/2$). Although the two endgames have similar costs, sequence of resonances and transfer time, they are significantly different in the region around the minor body, and they belongs to two different basins of attraction for the optimization problem in the CR3BP. This subtlety justifies the choice of optimizing both of them.

The trajectory optimization problem in the CR3BP is formulated as a nonlinear parameter optimization problem, where the dynamics constraints (equations of motion) are solved implicitly. The control variables

are the times, altitudes $r_\pi - \tilde{r}_M$, speeds V_π and angles θ of all the closest approaches and the times of the mid-course maneuvers.

The optimizer first propagates the states of every close approach backward and forward in time until the mid-course maneuvers time. The position of the last point of the forward propagation is then constrained to match the position of the last point of the backward propagation from the next closest approach*. The corresponding velocities are free but their difference, in norm, is added to the merit function.

As we are ultimately interested to compare the VILM solutions to the CR3BP endgame, we add constraints to fix the boundary conditions. In particular, we constrain the first closest approach to keep the first guess $\beta_{(i)}$ and v_∞, and we constrain the last closest approach to a given altitude and v_∞.

The first guess is generated using the VILM approach. The VILM solutions provide the times of the mid-course maneuvers and the flyby times, altitudes, and v_∞. Eq. (6), Eq. (9) , and Eq. (8) are used to compute the angles θ and the velocities V_π. Finally the parameter optimization problem is fed into the Matlab solver *fmincon*. For both endgames, Figure 2 shows the initial guesses (dash lines) and the optimized solutions (solid lines). The total cost of the optimized long-transfer endgame is 147 m/s (the VILM solution costs 154 m/s m/s), while the cost of the optimized short-transfer endgame is 165 m/s (the VILM solution costs 155 m/s).

Limitations of the VILM approach

The VILM approach is very fast and intuitive, and we envision using it for preliminary design of endgame and begingame trajectories whenever long- transfer time low-cost solutions are not an option. However the previous section showed that the VILM approach has some important limitations that deserve attention.

First, the cost of the VILM endgames can be off up to $\pm 5\%$ when compared to the more accurate CR3BP solutions†. We expect this error to increase as more resonances and high-altitude gravity assists are added.

Second, while the VILM approach estimates approximately the same Δv for the short-transfer solution and the long-transfer solution, the CR3BP shows that one kind of transfer is preferable (the long-transfer in the case shown in the previous section).

Finally, and most importantly , quasi-ballistic endgames cannot be found by simply designing a VILM endgame and optimizing it in the CR3BP. The linked-conic approach cannot explain the existence of ballistic endgames - not even in the limit of infinite transfer time where a minimum $\Delta v \neq 0$ can be computed.[9] In addition, the last chapter showed that the VILM solutions do not converge to quasi-ballistic endgames in the CR3BP. In fact the multi-resonant transfers are chaotic in nature where the design space is plagued by multiple local minima[6] that can easily trap gradient based optimizers. Clearly local minima exist in the CR3BP when using the VILM as an initial guess, but its unrealistic for the optimizer to climb out of that basin en route to quasi ballistic solutions. Instead we should seek solutions that start in the correct basin!

For the above reasons we seek to further our understanding of the dynamics of near ballistic endgame transfers. Ultimately, we seek systematic methods and tools to design such transfers. While the patched CR3BP is the first step towards solutions in a fully perturbed n-body model, the CR3BP indeed captures the dominant dynamics. Further, the system is Hamiltonian, allows for rapid computations, and preserves the Jacobi constant (or equivalently, in the case of this study, the Tisserand Parameter).

THE TISSERAND PARAMETER AND THE T-P GRAPH

In this section we introduce the T-P graph (named after Tisserand and Poincaré). The graph is a fundamental tool that provides dynamical justification for the Multi-Body technique and can be used to design quasi-ballistic transfers between moons. The T-P graph is built plotting Poincaré sections of different CR3BP models in one unique r_a, r_p graph. In the same graph the level sets of the respective Tisserand parameters are

*Because the problem is formulated in the rotating reference frame, the approach is robust despite the several revolutions (in the inertial frame) which occur between the flybys and the mid-course maneuvers.

†These values are consistent with the $\pm 10\%$ difference observed during the design of the Cassini tour when comparing Δv costs in the linked conics model with more accurate models (personal communication from Nathan Strange).

also plotted. The result is the T-P graph, which can be interpreted as an extension of the Tisserand graph[13,14] from the linked-conic model to the patched CR3BP model.

Poincaré Section

The first step in building the T-P graph is the introduction of a Poincaré section in the negative x-axis of the rotating reference frame of each CR3BP. When the spacecraft crosses the Poincaré section, far from the minor body, its trajectory is very well approximated by a Keplerian orbit around the major body. From the state vector at the crossing point we compute the osculating pericenter and apocenter relative to the main body, which we plot in a $r_a - r_p$ graph, similar to the one described in.[9] Figure 3 on the left shows a schematic of the Poincaré section and the corresponding $r_a - r_p$ graph.

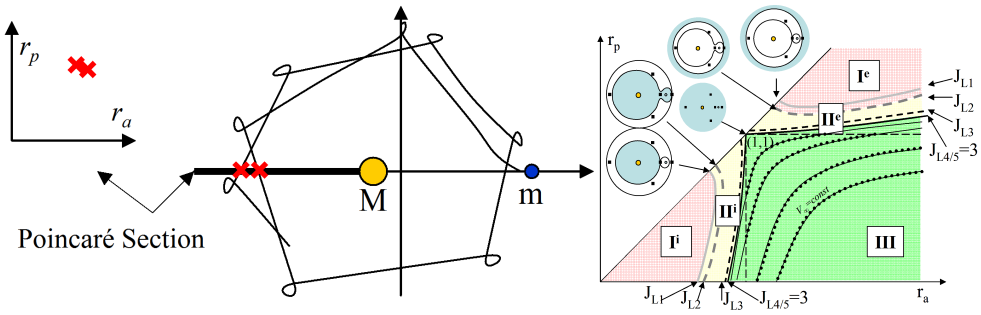

Figure 3 On the left, the Poincaré section for the definition of the T-P graph (schematic). On the right, Tisserand parameter level sets on the T-P graph and regions of motion in the CR3BP (schematic).

The Tisserand parameter

On the same graph we plot the level sets of constant Tisserand parameter . The Tisserand parameter T is a function of the semi-major axis a (in normalized units: $a = \tilde{a}/\tilde{a}_M$), inclination i and eccentricity e of a spacecraft orbiting a major body:[15]

$$T(a, e, i) = \frac{1}{a} + 2\sqrt{a\left(1 - e^2\right)}\cos i \tag{10}$$

In this work we consider the planar problem and rewrite Eq. (10) as function of the pericenter and apocenter only:

$$T(r_a, r_p) = \frac{2}{r_a + r_p} + 2\sqrt{\frac{2 r_a r_p}{r_a + r_p}} \tag{11}$$

The Tisserand parameter remains approximately constant even after a close encounter with a minor body. This is known as the *Tisserand criterion*.[15] It is well-known in fact that the Tisserand parameter is an approximation of the Jacobi constant J of the CR3BP, .i.e $T \approx J$.

The approximation is increasingly accurate for smaller mass parameters μ and when the spacecraft is far from the minor body (e.g. when it crosses the Poincaré section defined previously). In the appendix A2 we show how to derive the Tisserand parameter from the Jacobi constant; similar derivations are found in literature (see for example[16]).

The T-P graph

Now we are ready to plot the level sets of the Tisserand parameter onto the $r_a - r_p$ graph. We start plotting the four level sets $T = J_{Li}$, $i = 1, \ldots, 4$, where J_{Li} is the value of the Jacobi constant associated to the i^{th}

Lagrangian points (note that $J_{L4} = J_{L5} = 3$). The level sets divide the $r_a - r_p$ graph into regions of motion, as shown in Figure 3 on the right.

As the spacecraft crosses the Poincaré section, the osculating orbital elements are represented with a point on the T-P graph. If the point is in the region I^i, the spacecraft position is bounded in a region close to the major body and no transfer to the minor body is possible. Similarly, if the spacecraft is in the region I^e, the spacecraft is bounded in a region far from the major body and no transfer to the minor body is possible.

Transfers to the minor body are possible only when the spacecraft is in the regions II^i, II^e, III. In particular, we expect low-energy transfer and capture trajectories to occur in the region II^i (if coming from the inner moons) or II^e(if coming from the outer moons).

Note that inside the box $r_p < 1$, $r_a > 1$ (within region III) we can also plot the constant v_∞ level sets, as done in the Tisserand graph.[14] The v_∞-infinity level sets overlap with the constant Tisserand level sets*. In fact it can be proved that (see the appendix A2 and also[16]):

$$T = 3 - v_\infty^2 \approx J$$

We also include in the graph curves at constant resonance $n : m$ (where n is the number of body revolutions and m is the number of spacecraft revolutions), which are lines with slope -1:[9]

$$a = \left(\frac{n}{m}\right)^{2/3} \rightarrow r_p = -r_a + 2\left(\frac{n}{m}\right)^{2/3}$$

In order to study transfers between minor bodies, we plot on the same graph several Tisserand level sets, each in the dimensioned coordinates of the corresponding minor body. The Tisserand parameter with respect to the minor body M is:

$$T_M = \frac{2\tilde{a}_M}{\tilde{r}_a + \tilde{r}_p} + 2\sqrt{\frac{2\tilde{r}_a\tilde{r}_p}{(\tilde{r}_a + \tilde{r}_p)\,\tilde{a}_M}} \tag{12}$$

Finally we include a grid which shows the Δv required to change the pericenter/apocenter using an impulsive maneuver.

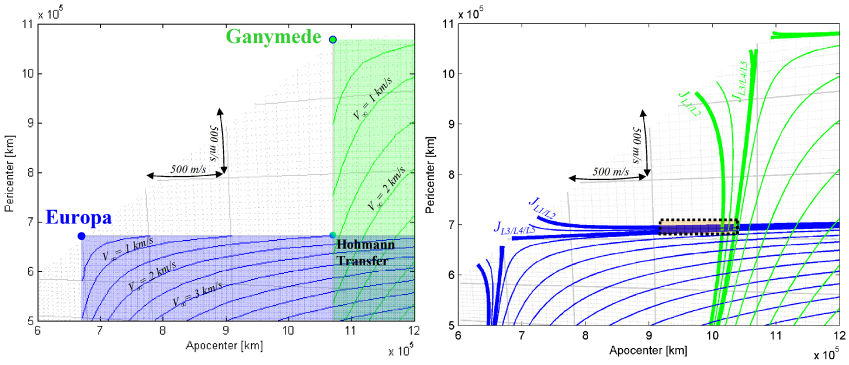

Figure 4. Tisserand Graph (on the left) and T-P graph (on the right).

The result is the T-P graph , which we show in Figure 4 on the right. In the same figure on the left, we plot the $r_a - r_p$ Tisserand graph explained in.[9] We see how the extension from a linked-conics model (for the Tisserand graph) to patched CR3BP model (T-P graph) results in level sets which extend over the feasible domain of the Tisserand graph. As a consequence, even low-energy (low v_∞) level sets reach very high apocenters.

*Then we can think of the Tisserand level sets as J level set or C3=v_∞^2 level sets

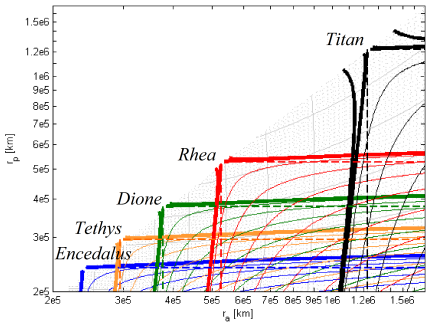

Figure 5. The T-P graph of the Saturn System.

Figure 5 shows the T-P graph for the Saturn system. We can see that the low-energy level sets (region II^e and II^i) of any two moons cross, in contrast to the linked conics model where ballistic intermoon transfers are only possible for v_∞ greater than that of the corresponding Hohmann transfer. From an *energetic* point of view, then, a ballistic transfer between any two moons in the patched CR3BP is always possible. This does not guarantee that such transfers can be found, especially within a practical transfer time. Some recent works demonstrate that such transfers can exist.[7]

The intersection point between the Tisserand level sets of two different moons is the solution of the system:

$$\begin{cases} T_{M1} &= \frac{2\tilde{a}_{M1}}{\tilde{r}_a+\tilde{r}_p} + 2\sqrt{\frac{2\tilde{r}_a\tilde{r}_p}{(\tilde{r}_a+\tilde{r}_p)\tilde{a}_{M1}}} \\ T_{M2} &= \frac{2\tilde{a}_{M2}}{\tilde{r}_a+\tilde{r}_p} + 2\sqrt{\frac{2\tilde{r}_a\tilde{r}_p}{(\tilde{r}_a+\tilde{r}_p)\tilde{a}_{M2}}} \end{cases} \tag{13}$$

where we solve for r_a, r_p giving the desired T_{M1} and T_{M2} along with the $\tilde{a}_{M1}$ and $\tilde{a}_{M2}$ for the systems of interest. We emphasize that the T-P graph provides a reliable energetic based strategy to patch the two CR3BP systems. The patch point target provides a significant advantage over prior multi-body design methodologies.

Three-dimensional T-P graph

In this section we consider the 3D case, where the Tisserand parameter is function of the apocenter, the pericenter, and the inclination:

$$T_M = \frac{2\tilde{a}_M}{\tilde{r}_a+\tilde{r}_p} + 2\sqrt{\frac{2\tilde{r}_a\tilde{r}_p}{\tilde{r}_a+\tilde{r}_p}}\cos i \tag{14}$$

The 3D T-P graph can be used to visualize families of asteroids in the solar system,[17] or to analyze missions like the Solar Orbiter which uses resonant gravity assists at Venus to reach high inclinations over the ecliptic.[18] Figure 6 on the top shows the Earth and Jupiter Tisserand level sets, and the main-belt asteroids. Most of the main-belt asteroids are outside the surfaces $T_{Earth} = J_{L1Earth}$ and $T_{Jupiter} = J_{L1Jupiter}$. We also can see the Kirkwood gaps at the resonances $1:4$, $3:1$, $2:5$, and $1:2$ (see for instance[19]). Figure 6 on the bottom shows the Near Earth Asteroids and, among those, the Potentially Hazardous Asteroids. We can see the Potentially Hazardous Asteroids are all within the level set $T_{Earth} = J_{L1Earth}$.

THE ANATOMY OF THE MULTI-BODY TECHNIQUE

In this section we use the T-P graph to explain how the Multi-Body Techniques are used to design endgame trajectories.

The Multi-Body Techniques propagate the state of the spacecraft in multi-body dynamics, targeting high altitude encounters with a minor body to achieve the most suitable effect (typically a reduction or an increase

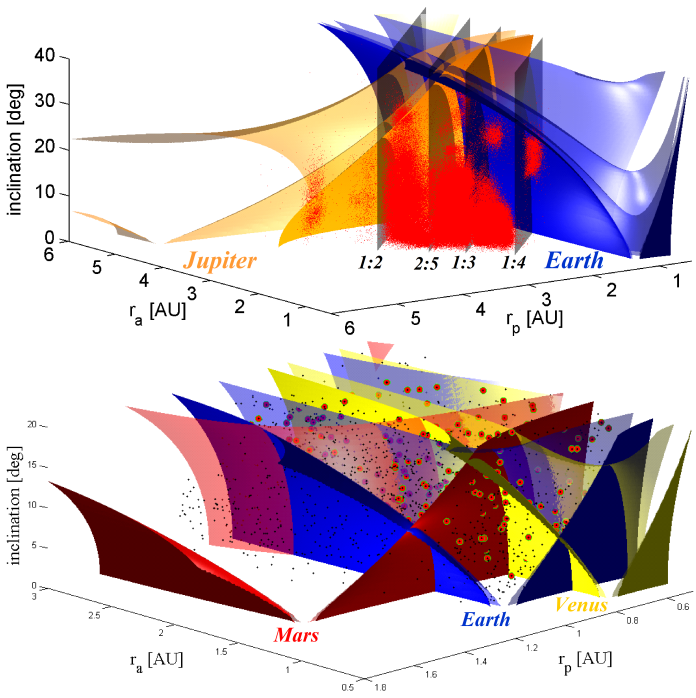

Figure 6 Examples of 3D T-P graph. On the top, the Earth and Jupiter level sets and the main -belt asteroids. On the bottom, the Near Earth Asteroids and, among those, the Potentially Hazardous Asteroids.

of the one of the apses). Trajectories designed with Multi-Body Techniques include the Smart1 mission to the Moon[5] , and the Multi-Moon Orbiter by Ross and Lo.[4]

The Multi-Moon Orbiter

The Multi-Moon Orbiter is a trajectory designed by Ross and Lo[4] for a mission to the Jovian moons. Figure 7 on the left shows the trajectory (picture taken from[4]) in the inertial, Jupiter-centered reference frame. The trajectory was computed in the planar, restricted 5 body problem.

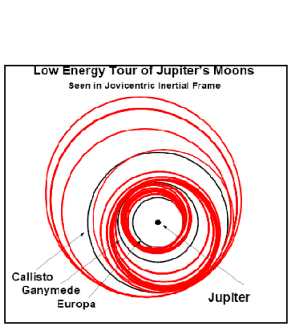

Picture from Shane&Lo

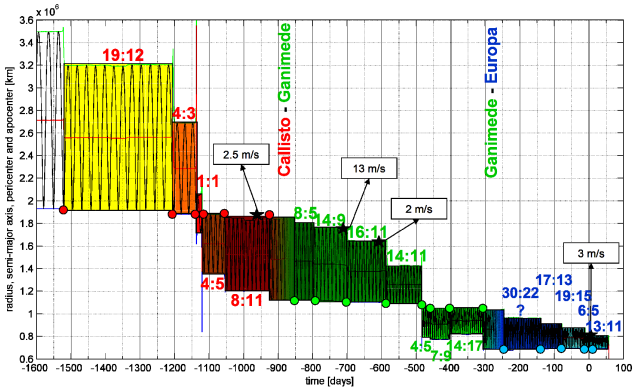

Figure 7 The MultiMoon Orbiter.[4] On the left, the trajectory in the inertial reference frame from the original paper. On the right, the radius and the osculating parameters as function of time.

Figure 7 on the right shows the radius and the osculating pericenter, apocenter, and semi-major axis of the

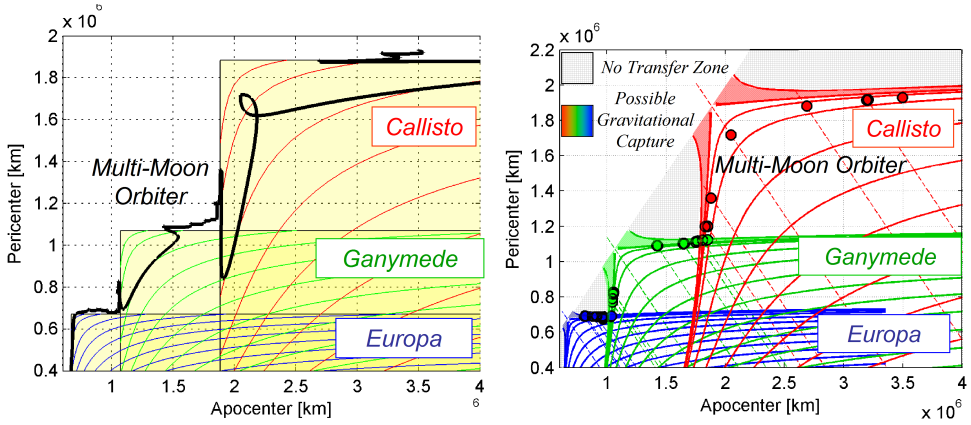

Figure 8 The MultiMoon Orbiter.[4] On the left, the trajectory osculating parameters are plotted in the (ra,rp) conventional Tisserand graph. On the right the same trajectory is represented with the T-P graph. The T-P graphs shows that the trajectory jumps between resonances and is mostly ballistic. We can see the no-transfer zones (light gray) and the capture zones. At the end of the trajectory, the spacecraft is inside the Europa capture zone.

trajectory as function of time. Figure 8 on the left shows the corresponding Tisserand graph in the Jupiter system. The orbital elements vary mostly during short time intervals when the spacecraft approaches a moon, making the Tisserand graph not easy to read. Also, the osculating pericenter and apocenter are often outside the boundaries ($\tilde{r}_a > \tilde{r}_M$, $\tilde{r}_p < \tilde{r}_M$) imposed by the linked-conic model.

We now represent the same trajectory with the T-P graph. We first split the trajectory in three parts, depending on the dominating perturbing body. The first part is dominated by Callisto, the second by Ganymede and the third by Europa. For each part we place a Poincaré section on the negative x-axis of the corresponding rotating reference frame, and build the T-P graph of the transfer. The result is shown in Figure 8 on the right. We see that the spacecraft jumps between resonant orbits using flybys at the moons. Although Ross and Lo's trajectory was computed in the restricted 5 body problem, Figure 8 shows that the patched CR3BP model is a good approximation and that the T-P graph captures the main dynamics; in fact the spacecraft first shadows the T_M level sets of Callisto, then of Ganymede, and finally of Europa. The T-P graph also shows that the trajectory is quasi-ballistic*.

The ballistic endgame paradox

Endgame or transfer trajectories designed with the linked-conic model always require some impulsive maneuver (Δv). The Δv is needed to increase/decrease the v_∞ from the escape/capture condition because in general the departure/arrival low-energy (low V_∞) level sets do not intersect (see left side of Figure 4). To decrease the required Δv, a VILM strategy can be implemented using a sequence of almost resonant orbits and small maneuvers (i.e. a zig-zag path in the $r_a - r_p$ leveraging graph). For very long transfer times a theoretical minimum Δv can be computed.[9]

In the patched CR3BP model the T-P graph shows that the same low-energy (high Tisserand) level sets do indeed intersect. Then there might be endgames and transfers between moons which require little or no Δv, and which consist of resonant orbits only; in fact, the Multi-Moon Orbiter trajectory[4] is one example of such a transfer.

Yet an interesting paradox arises when considering *planar* ballistic endgames:

> Given a fixed Tisserand energy and arrival circular orbit altitude, the insertion maneuver costs remain essentially fixed for all possible arrival geometries.

*Another ballistic transfer is explained with the T-P graph in the Saturn-Titan system in[20]

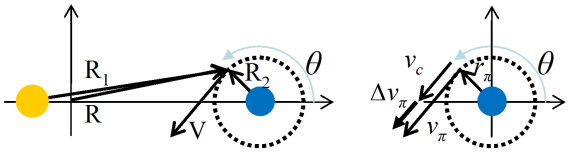

Figure 9. Possible orbit insertion locations at the end of an endgame strategy.

The paradox seems to questions the utility of resonant orbits, and of quasi-ballistic endgames in general. In what follows we first prove the paradox, and then we explain why resonant orbits are still necessary for the design of low-energy endgames.

Assume a ballistic endgame begins at Europa with a very high apocenter (for example in the region II^e), and ultimately targets a low altitude circular orbit (e.g. 100 km) at Europa. In the planar case, the orbit insertion location is somewhere on a circle of radius $R_2 = r_\pi$ around Europa. Figure 9 shows the possible orbit insertion locations as function of the angle θ. On the left, the arrival conditions are represented in the rotating reference frame; on the right the arrival conditions and the orbit insertion maneuvers Δv_π are represented in the inertial, moon-centered reference frame.

We now compute the orbit insertion maneuver as a function of the angle θ, for a given Jacobi constant and altitude at the moon. From simple geometric considerations:

$$R_1 = \sqrt{1 + r_\pi^2 + 2r_\pi \cos\theta} \tag{15}$$

$$R^2 = (1-\mu)^2 + r_\pi^2 + 2(1-\mu) r_\pi \cos\theta \tag{16}$$

Substituting Eq.(15) and Eq.(16) in Eq.(4) we find that the velocity in the rotating frame is:

$$V^2 = (1-\mu) + r_\pi^2 + 2(1-\mu) r_\pi \cos\theta + 2\frac{1-\mu}{\sqrt{1 + r_\pi^2 + 2r_\pi \cos\theta}} + 2\frac{\mu}{r_\pi} - J \tag{17}$$

The velocity in the inertial frame is (see appendix A1):

$$v_\pi = (V + \sigma r_\pi) \tag{18}$$

The orbit insertion/escape Δv is:

$$\Delta v_\pi = v_\pi - v_c = V + \sigma r_\pi - v_c \tag{19}$$

where $v_c = \sqrt{\mu / r_\pi}$. Then the orbit insertion cost depends on V. It is easy to prove that $V^2(\theta)$ has a global maximum at $\theta = 0$ and a global minimum at $\theta = \theta^* = \arccos(-r_\pi/2)$. Also, $\left(V^2\right)_{MAX} - \left(V^2\right)_{MIN} = r_\pi^2 (1-\mu) \frac{3+r_\pi}{1+r_\pi}$, and because r_π^2 is small compared to other terms in Eq. (17) we infer that $V_{MAX} \approx V_{MIN}$, i.e. the velocity and thus the orbit insertion maneuver doesn't depend significantly on the angle θ.* Table (1) shows $(\Delta v_\pi)_{MAX}$ and $(\Delta v_\pi)_{MIN}$, computed for θ =0 and $\theta = \theta^*$ respectively, for several cases of interest. We see that in all cases the difference in the orbit insertion maneuver is just a few meters per seconds or less, thus given a fixed energy a ballistic endgame (which can only change θ) cannot reduce the cost significantly†.

The paradox seems to question the utility of the ballistic endgame, at least in the planar case, because no matter how we design a sequence of resonant orbits, the orbit insertion Δv is fixed by the Jacobi constant and cannot change. We wonder then why we need resonant transfers in the first place.

*It would be interesting to know if the paradox extends to the 3D case, where $R^2 = 1 + r_\pi^2 \cos^2\alpha + 2r_\pi \cos\theta \cos\alpha$, $R_1 = \sqrt{1 + r_\pi^2 + 2r_\pi \cos\theta \cos\alpha}$ and α is the elevation angle on the xy plane. The velocity in the inertial frame has two components, i.e. V and $\omega \times r$, which are not aligned in general.

†Non-ballistic endgame can reduce the orbit insertion maneuver by applying impulsive Δv which results in the highest change in the Jacobi constant. The VILM strategy can be justified with this argument also[21]

Moon	$\Delta v_{MAX}/\Delta v_{MIN}$ (km/s)			
	J_{L1}@100km	J_{L4}@100km	J_{L1}@1000km	J_{L4}@1000km
Europa	421.1/420.1	606.5/605.5	276.7/273.7	513.7/511.1
Titan	668.6/668.5	766.5/776.4	553.7/553.5	667.6/667.5

Table 1 The maximum and minimum orbit insertion maneuver (m/s) for given altitudes and Jacobi constant at Europa and at Titan.

The T-P graph clarifies this point, and enables strategies for the design of low-cost, quasi-ballistic endgames and transfers. A low-cost , quasi-ballistic endgame at Europa, e.g., must end with a low Δv orbit insertion. Referring to Figure 3 on the right, the corresponding T level sets will probably lie within region II^e. Because the endgame is quasi-ballistic, the initial conditions also lie in the region II^e and according to the boundaries of the region II^e in Figure 4, an initial high apocenter requires an initial high pericenter, beyond Europa's orbit. How can the spacecraft, then, ever reach a 100 km altitude to Europa, an impossible scenario based on the conventional wisdom of linked-conics? The T-P graph shows, however, that if the spacecraft has the right phasing, it can use Europa perturbing force to slightly lower its apocenter AND pericenter, thus moving to the left in the T-P graph, along the level set.

Such maneuver is in fact a high altitude flyby performed close to the pericenter of the spacecraft orbit. When several high altitude flybys are linked together by free-return orbits, the pericenter can be lowered to the point where a 100 km approach at Europa is possible. Thus the high altitude flybys are necessary *to reduce the pericenter* and to reach the required altitude at Europa, while the resonant orbits simply provide a mechanism to achieve multiple flybys. We note that energy levels of the endgame scenario require non intersecting spacecraft and minor body orbits (in the exterior problem the spacecraft orbit engulfs completely the orbit of the minor body for all time while the interior problem is reversed). Therefore, the point of closest approach for the two orbits occurs only at a single point in the nonrotating frame: the apse of the spacecraft orbit. Accordingly, the low-cost endgame return orbit must be approximately resonant; whereas a non-resonant returns would necessarily have two intersection points between the spacecraft and minor body orbits.

An alternative way to explain the ballistic endgame is the following: of all the trajectories arriving at 100 km altitude at Europa with a fixed velocity defined by Eq.(18), the only one which starts at a very high apocenter must have performed several high altitude flybys and resonant orbits. In the next section we use this concept to design ballistic transfers.

THE DESIGN OF MULTI-BODY TRANSFERS WITH THE T-P GRAPH

The previous section showed that even for low energy levels (i.e. Tisserand parameter between J_{L1} and 3) there can be trajectories which reach a low altitude at a moon, starting at a very high apocenter, through a sequence of flybys and resonant orbits. In this section we implement a simple search to find such trajectories and design low-cost transfers between Ganymede and Europa. A similar search was implemented in the design of the BepiColombo capture trajectory at Mercury;[22] in fact at these energy levels many ballistic capture or escape trajectories can be designed.[23,24,25]

We first design a transfer between a 100 km altitude orbit at Ganymede and a 100 km altitude orbit at Europa. A direct Hohmann transfer would require only a few days, but would cost 2.18 km/s. A VILM strategy can reduce this Δv to a theoretical minimum of 1.71 km/s. Using the T-P graph and the higher fidelity CR3BP, we demonstrate how a low-cost transfer can require significantly less propellant.

The basic scheme for the design is shown in Figure 10. We start by fixing an energy value for the escape and for the capture such that the spacecraft starts in the "escape region" II^e and ends in the "capture region" II^i. In particular, we choose

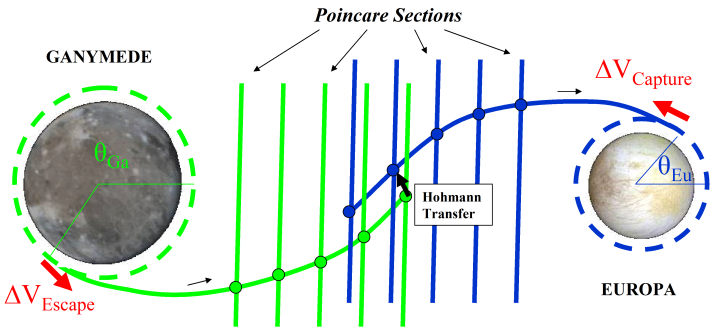

Figure 10. Schematic of a transfer between Europa and Ganymede designed using the T-P graph.

$$T \approx J = (J_{L2} + J_{L3})/2 \tag{20}$$

From the Jacobi constants we find the velocities at pericenter using Eq. (18)*, and calculate the cost to insert into/escape from a circular orbit at 100 km altitude from Eq.(19) : $\Delta v_{Escape} \cong 0.72$ km/s and a $\Delta v_{Capture} \cong 0.51$ km/s. Immediately we see that the floor for a potentially ballistic transfer Δv is $\Delta v_{Escape} + \Delta v_{Capture}$. We then scan the angles θ_{Ga}, propagate the initial conditions and store the transfers that decrease the pericenter the most in the shortest time. We also scan the angles θ_{Eu}, propagate *backwards* the initial conditions and store the transfers that increase the apocenter the most in the shortest time. In both the forward and backward propagations we have a precalculated target value for r_a and r_p respectively - from the intersection point in the TP graph - found from the solution to Eq. (13).

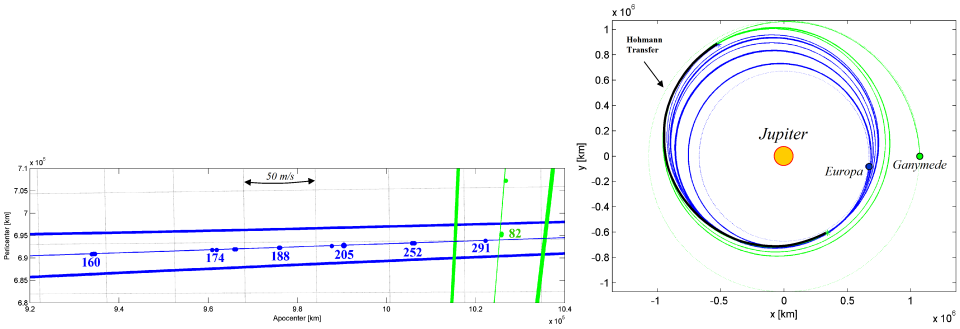

Figure 11 Left: Zoom of the T-P graph showing the Ganymede escape options and the Europa capture options. Right: Quasi-ballistic transfer in the inertial reference frame.

We plot the results in the T-P graph. A close up is shown in Figure 11 on the left. In the graph we plot the level sets corresponding to the value of the Tisserand parameter in Eq. (20). One of the most important features of the T-P graph is the availability of a target pericenter-apocenter for both endgame and begingame strategies, which is at the intersection of the level sets. For clarity we do not plot all the Poincaré crossings from all the trajectories; we only plot the set of Pareto-optimum points (shortest time, highest apocenter) reached by all the solutions. Note that the final points of the begingame and the initial points of the endgame do not coincide in general. Thus some impulsive maneuvers are needed to patch the two parts of the transfer; the grid in the T-P graph provides a means to estimate a brute force patching cost of a Hohmann-like transfer to connect the points in the graph. For instance we can estimate a Δv of some 70 m/s to patch the 82 day begingame with a 252 day endgame.

*In this example we do not consider the retrograde solution.

Among all the possible solutions on the graph, we choose the one with lower Δv which takes $(291 + 82)$ days to transfer from Ganymede to Europa. In this case the T-P graph shows that a very little Δv (approx.10 m/s) is required to patch the begingame with the endgame. Then the total cost of the transfer (to and from 100 km circular orbits) is mostly given by the escape and capture maneuver for a $\Delta v_{TOT} \approx 1.25$ km/s, almost 500 m/s less than the VILM theoretical minimum Δv , and almost 1 km/s less (but one year more!) than the direct Hohmann transfer.

Figure 12 shows the begingame and the endgame part of this trajectory in the corresponding rotating reference frames. Figure 11 on the right shows the same trajectories in the inertial reference frame centered at Jupiter. The figure also shows the Hohmann transfer which patches the two parts of the trajectory.

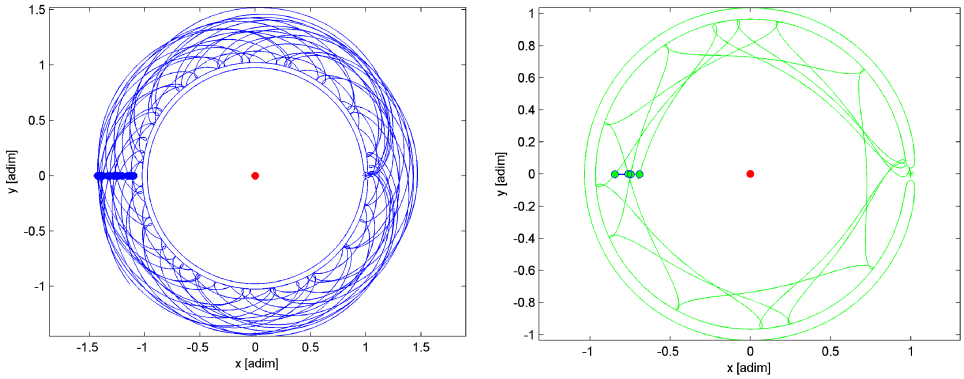

Figure 12 Quasi-ballistic transfer in the rotating reference frame. On the left, the endgame at Europa. On the right, the begingame at Ganymede.

A more interesting case for a real mission is the transfer between a halo orbit around Europa and a halo orbit around Ganymede. In this case the orbit insertion Δv and the orbit escape Δv are negligible, and the long transfer time is justified by a fully quasi-ballistic transfer. The trajectories are computed in the patched , spatial CR3BP, and the inclination at the Poincaré section never exceeds 1.5 degree.

To find suitable transfers we scan the initial position along the initial and final halo orbits and perturb the starting conditions along the unstable and stable eigendirection respectively. The initial halo orbit has a Jacobi constant in the Jupiter-Ganymede CR3BP of J=3.0052, and the final halo orbit has a Jacobi constant in the Jupiter-Europa CR3BP of J=3.0023. The energy levels are selected to be appropriate for ballistic transfers to a high altitude closed orbits about each moon.[26]

Of all the solutions found, we show one with a reasonably low flight time and comes close to hitting the target (r_a, r_p) intersection of $(694641\ km,\ 1021834\ km)$, found from the solution to Eq. (13). Figure 13 shows the T-P graph at $i = 0$ of the begingame and of the endgame. For simplicity, the osculating pericenter

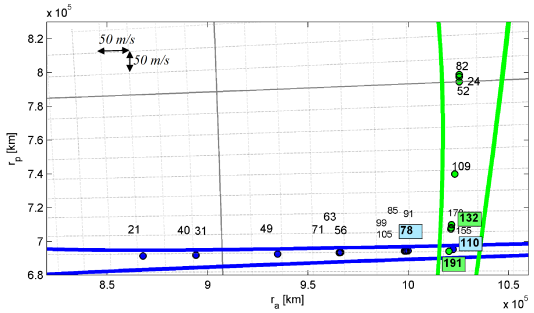

Figure 13 T-P graph of the transfer from a halo orbit around Ganymede to a halo orbit around Europa - projection onto the $i = 0$ plane.

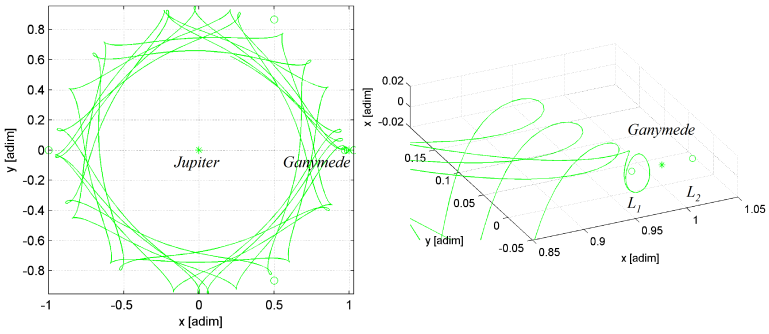

Figure 14 Begingame at Ganymede, the first part of the Ganymede to Europa transfer, in the rotating reference frame.

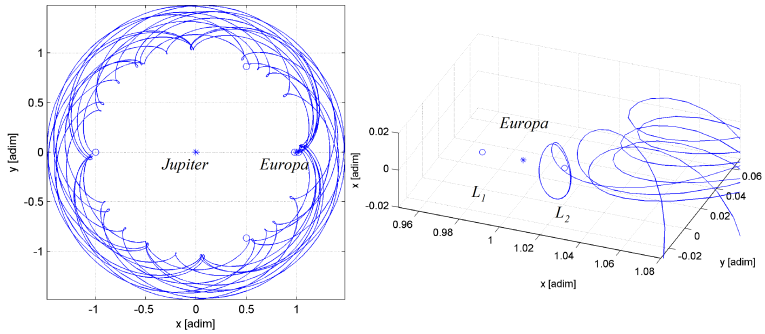

Figure 15 Endgame at Europa, the second part of the Ganymede to Europa transfer, in the rotating reference frame.

and apocenter and inclination at the Poincaré section are projected on the $i = 0$ plane (we recall that the inclination never exceeds 1.5 degrees) . The Ganymede begingame takes 191 days to reach a very low pericenter, where it can be patched to the Europa endgame with a very little Δv. The endgame lasts 110 days. Then the whole transfer takes less than 300 days (some initial revolutions are spent on the initial and final halos) and from the T-P graph we see that almost no Δv is required to patch the two trajectories. Note that the begingame could be reduced by two months with some additional 50 m/s , resulting in a 8-month transfer from Ganymede to Europa. Also, the begingame can be reduced by one moth with some additional 50 m/s, resulting in a 7-month transfer which costs some 100 m/s.

The next figures show some details of the 300-day transfer. Figure 14 shows the begingame in the Jupiter-Ganymede CR3BP , with a close up of the escape from the halo orbit. Figure 15 shows the endgame in the Jupiter-Europa CR3BP, with a close up of the capture into the halo orbit. In total there are 3 high altitude flybys of Ganymede and 6 high altitude flybys of Europa.

In future works we plan to optimize this trajectory or similar ones in the full ephemeris model. We do not expect the transfer time of the full-ephemeris trajectory to differ too much from the estimated value on the T-P graph. The total Δv might vary due to two important factors. On one hand the Δv can increase due to change of plane maneuvers and fourth body perturbations. On the other hand we can reduce the Δv by inserting several mid-course maneuvers along the trajectory and using an optimizer to minimize the total cost. Also we can reduce the Δv by fine-tuning the initial and final energies. Future works could also include explicit VILM-type maneuvers to shorter the time of flight of low-energy transfers.

We emphasize that the design approach outlined in this study requires no apriori knowledge of the resonant path and relies only the chaotic nature of the CR3BP and fine-scale perturbations of the initial conditions. Future work includes methods that allow specification of the resonant paths to reduce the computation re-

quirements and provide more systematic searches. Recent works in the field also suggest some ways to achieve this goal.[8]

CONCLUSION

In this paper we present a new graphic tool, the T-P graph, to understand and design low-cost endgames and transfers - in the context of both linked-conics and patched three body systems. While the T-P graph can be used like the Tisserand graph, it extends beyond the limits of the linked-conic approach into the domain of the patched CR3BP showing that low-energy ballistic orbits around the moons are energetically connected. The T-P graph also provides target points and a simple rationale for the design of such transfers.

With a very simple search, we designed a transfer between a circular orbit at Europa and a circular orbit at Ganymede which requires only 1.25 km/s, almost 500 m/s less than the theoretical minimum cost achieved by VILM transfers, and almost 1 km/s less that the direct Hohmann transfer. With the same approach we found a transfer between a halo orbit around L1 of the Ganymede-Jupiter system and a halo orbit around L2 of the Europa-Jupiter system. The transfer is quasi-ballistic and lasts 300 days, and can be shortened by two months for an additional 50 m/s, or by three months by an additional 100 m/s.

In the future we plan to optimize these trajectories in the ephemeris model. The total Δv could decrease because of the optimization or increase due the effects which were neglected in the patched CR3BP. Many more solutions can be found using simple search approaches, however we also envision using other more systematic techniques that use the TP graph to design and patch resonant orbits, high altitude flybys, and small mid-course maneuvers. Ideally we would like to short the transfer times using VILM-type maneuvers in the patched CR3BP.

ACKNOWLEDGMENT

The authors would like to thank Jon Sims (JPL), Nathan Strange (JPL), Anastassios Petropoulos (JPL), Arnaud Boutonnet (ESA), Shane Ross (VirginiaTech), Martin Gehler (RWTH Aachen Univeristy), and Evan Gawlik (Caltech) for their valuable comments.

NOTATION

$\tilde{x}$	Tilde indicates dimensional variable.
X, x	Upper case for variables in the rotating frame, lower case for variables in the inertial frame.
P	Subscript indicates the quantity is referred to the major body.
M	Subscript indicates the quantity is referred to the minor body.
T	Tisserand Parameter
J	Jacobi constant
v_∞	Relative velocity of the spacecraft at the minor body.
r_π, v_π	Position and velocity of the spacecraft with respect to the minor body at the closest approach
a, e, i	Semi-major axis. eccentricity, inclination with respect to the major body
r_a, r_p	Pericenter, apocenter with respect to the major body
μ	Gravitational constant.

REFERENCES

[1] J. R. Johannesen and L. A. D'Amario, "Europa Orbiter Mission Trajectory Design," *AAS 99-360*, 1999.

[2] G. Hollenbeck, "New Flight Techniques for Outer Planet Missions," *AAS Paper 75-087 AIAA/AAS Astrodynamics Specialist Conference, Nassau, Bahamas, July 1975*, 1975.

[3] J. A. Sims, J. M. Longuski, and A. Staugler, "V-infinity Leveraging for Interplanetary Missions: Multiple-Revolution Orbit Techniques," *Journal of Guidance, Control and Dynamics*, Vol. 20 n 3, 1997, pp. 409–415.

[4] S. D. Ross and M. W. Lo, "Design of a Multi-Moon Orbiter," *Paper AAS 03-143, AAS/AIAA Space Flight Mechanics Meeting, 9-13 February 2003, Puerto Rico*, 2003.

[5] J. Schoenmaekers, J. Pulido, and J. Cano, "SMART-1 Moon mission: trajectory design using the Moon gravity," tech. rep., ESA, ESOC, SI-ESC-RP-5501, 1999.

[6] S. D. Ross and D. J. Scheeres, "Multiple Gravity Assist, Capture and Escape in the Restricted Three-Body Problem," *SIAM Journal on Applied Dynamical Systems*, Vol. 6 n 3, 2007, pp. 576–596.

[7] S. D. Ross, S. Jerg, and O. Junge, "Optimal Capture Trajectories Using Multiple Gravity Assists," *Communications in Nonlinear Science and Numerical Simulations*, 2009. [in press].

[8] P. Grover and S. D. Ross, "Designing Trajectories in a Planet-Moon Environment Using the Controlled Keplerian Map," *Journal of Guidance, Control, and Dynamics*, [accepted].

[9] S. Campagnola and R. P. Russell, "The Endgame Problem Part A: V-Infinity Leveraging Technique and the Leveraging Graph," *Proceedings of the 2009 AIAA/AAS Space Flight Mechanics Meeting*, 2009.

[10] A. Boutonnet, P. d. Pascale, and E. Canalias, "Desing of the Laplace Mission," *Paper IAC-08-C1.6, 59th IAC, Glasgow, Scottland*, 2008.

[11] V. Szebehely, *Theory of orbits. The restricted problem of three bodies*. New York: Academic Press, 1967.

[12] H. Poincaré, *Les Méthodes Nouvelles de la Mécanique Celeste*. Paris, Gauthier-Villars et fils, 1892.

[13] A. Labunsky, O. Papkov, and K. Sukhanov, *Multiple Gravity Assist Interplanetary Trajectories*. Earth Space Institute Book Series, Gordon and Breach Publishers, London, 1998.

[14] N. J. Strange and J. M. Longuski, "Graphical Method for Gravity-Assist Trajectory Design," *Journal of Spacecraft and Rockets*, Vol. 39, N. 1, 2002, pp. 9–16.

[15] F. F. Tisserand, *Traite' de Mechanique Celeste*, Vol. 4. Gauthier-Villars et fils, 1896.

[16] J. K. Miller and C. J. Weeks, "Application of Tisserand's Criterion to the Design of Gravity Assist Trajectories," *AIAA 2002-4717 AAS/AIAA Astrodynamics Specialist Conference and Exhibit, Monterey, GA, August 2002*, 2002.

[17] M. Gehler, "On Transport and Collision of Near Earth Objects Using Restricted Dynamical Systems; Diplomarbeit (Diploma Thesis - in preparation)," tech. rep., Institute of Aeronautics and Astronautics, RWTH Aachen University, 2009.

[18] G. Janin, A. Boutonnet, and S. Campagnola, "Solar Orbiter Mission Analysis," tech. rep., ESA, ESOC, WP 481, March 2005.

[19] C. D. Murray and S. F. Dermott, *Solar System Dynamics*. Cambridge University Press, February 2000.

[20] E. S. Gawlik, J. E. Marsden, S. Campagnola, and A. Moore, "Invariant Manifolds, Discrete Mechanics, and Trajectory Design for a Mission to Titan," *AAS 09-226, AAS/AIAA Space Flight Mechanics Meeting, Savannah, GA, Feb 2009*, 2009.

[21] T. H. Sweetser, "Jacobi's Intergal and DeltaV Gravity Assist (DeltaV EGA Trajectories)," *AAS 93-635 AIAA/AAS Astrodynamic Specialist Conference, Victoria, BC, Canada, Aug*, 1993.

[22] R. Jehn, S. Campagnola, D. Garcia, and S. Kemble, "Low-Thrust Approach and Gravitational Capture at Mercury," *18th International Symposium on Space Flight Dynamics*, Vol. 548 of *ESA Special Publication*, 2004, p. 487.

[23] S. Campagnola and M. W. Lo, "BepiColombo Gravitational Capture and the Elliptic Restricted Three-Body Problem," *Proceedings in Applied Mathematics and Mechanics*, 2007.

[24] M. E. Paskowitz and D. J. Scheeres, "Robust Capture and Transfer Trajectories for Planetary Satellite Orbiters," *Journal of Guidance, Control, and Dynamics*, Vol. 29, N. 2, 2006, pp. 342–353.

[25] B. F. Villac and D. J. Scheeres, "Escaping Trajectories in the Hill three Body problem and application," *Journal of Guidance, Control and Dyanmics*, Vol. 26, 2003, pp. 224–232.

[26] R. P. Russell and T. Lam, "Designing Ephemeris Capture Trajectories at Europa Using Unstable Periodic Orbits," *Journal of Guidance, Control and Dyanmics*, Vol. 30, No. 2, 2007, pp. p. 482 – 491.

[27] R. L. Anderson, *Low Thrust Trajectory Design for Resonant Flybys and Captures Using Invariant Manifolds*. PhD thesis, University of Colorado at Boulder, 2005.

APPENDIX A1: COORDINATE TRANSFORMATIONS

In this appendix we recall the coordinate transformations for the CR3BP and some useful expressions used in the paper. The steps are standard and can be found in literature (for example, a very clear explanation is in[27]) .

We start recalling the coordinate transformation from the rotating reference frame centered in the barycenter, to the inertial reference frame centered in either body. We define the state vector in the rotating frame:

$$S = \left(X, Y, Z, \dot{X}, \dot{Y}, \dot{Z}\right)^T \tag{21}$$

the state vector in the inertial reference frame, centered in the barycenter:

$$s_{(B)} = \left(x_{(B)}, y_{(B)}, z_{(B)}, \dot{x}_{(B)}, \dot{y}_{(B)}, \dot{z}_{(B)}\right)^T \tag{22}$$

the state vector in the inertial reference frame, centered in either body:

$$s = (x, y, z, \dot{x}, \dot{y}, \dot{z})^T \tag{23}$$

We recall that the all the variables are normalized using the scale factors defined in the paper, so that the angular velocity of the rotating frame is 1. Assuming the rotating frame has no initial phase w.r.t. the inertial frame, the transformation from S to $s_{(B)}$ is given by:

$$s_{(B)} = \left(X, Y, Z, \dot{X} - Y, \dot{Y} + X, \dot{Z}\right)^T \tag{24}$$

The transformation from $s_{(B)}$ to s is given by:

$$s = \left(x_{(B)} - d, y_{(B)}, z_{(B)}, \dot{x}_{(B)}, \dot{y}_{(B)} - d, \dot{z}\right)^T \tag{25}$$

where $d = -\mu$ if the inertial reference frame is centered in the major body, and $d = 1 - \mu$ if the inertial reference frame is centered in the minor body.

Thus the transformation from the rotating reference frame to the body-centered inertial reference frame and viceversa is given by the following equations:

$$(x, y, z, \dot{x}, \dot{y}, \dot{z})^T = \left(X - d, Y, Z, \dot{X} - Y, \dot{Y} - (X - d), \dot{Z}\right)^T \tag{26}$$

$$\left(X, Y, Z, \dot{X}, \dot{Y}, \dot{Z}\right)^T = (x + d, y, z, \dot{x} + y, \dot{y} - x, \dot{z})^T \tag{27}$$

In our work we are interested in the velocities in both reference frames. We first recall that the components of the velocity in the major/minor body reference frame are related to the magnitude of the angular momentum and inclination of the spacecraft w.r.t to the major/minor body through:

$$\dot{y}x - \dot{x}y = h \cos i \tag{28}$$

We use Eq.(27) and Eq. (28) to derive the an expression for the square of the velocity V^2:

$$V^2 = \dot{X} + \dot{Y} + \dot{Z} = (\dot{x} + y)^2 + (\dot{y} - x)^2 + \dot{z}^2 = v^2 + \left(x^2 + y^2\right) - 2h \cos i \tag{29}$$

Now we consider the special case in which :

$$s = (r_\pi \cos\theta, r_\pi \sin\theta, 0, -\sigma v_\pi \sin\theta, \sigma v_\pi \cos\theta, 0) \tag{30}$$

where $\sigma = +1$ for direct orbits and $\sigma = -1$ for retrograde orbits, and $r_\pi = R_2$ is the distance from the minor body.

Applying Eq. (27):

$$S = ((1-\mu) + r_\pi \cos\theta, r_\pi \sin\theta, 0, -(\sigma v_\pi - r_\pi)\sin\theta, (\sigma v_\pi - r_\pi)\cos\theta, 0) \tag{31}$$

so that

$$V = |\sigma v_\pi - r_\pi| = |v_\pi - \sigma r_\pi| \tag{32}$$

Assuming $v_\pi > r_\pi$, we find:

$$V = v_\pi - \sigma r_\pi \quad , \quad v_\pi = V + \sigma r_\pi \tag{33}$$

APPENDIX A2 : TISSERAND PARAMETER, JACOBI CONSTANT, AND VINFINITY

For completeness, In this appendix we derive the Tisserand parameter from the Jacobi constant. Similar derivations can be found in literature.[16]

Using Eq.(27) and Eq. (29) we express the Jacobi constant in the inertial reference frame centered in the major body:

$$J = \left((x-\mu)^2 + y^2\right) + 2\frac{1-\mu}{r} + 2\frac{\mu}{R_2} + (1-\mu)\,\mu - v^2 - r^2 + 2h\cos i \tag{34}$$

Using the *vis-viva* equation and the expression for the angular momentum

$$v^2 = 2\frac{1-\mu}{r} - \frac{1-\mu}{a} \tag{35}$$

$$h = \sqrt{a\,(1-e^2)\,(1-\mu)} \tag{36}$$

we find:

$$J = \frac{1-\mu}{a} + 2\sqrt{a\,(1-e^2)\,(1-\mu)}\cos i + 2\frac{\mu}{R_2} - x\mu + \mu^2 + (1-\mu)\,\mu \tag{37}$$

If we let $\mu \to 0$, and assuming R_2 is not too small (as in the case when far from the minor body), Eq. (37) becomes:

$$J \approx \frac{1}{a} + 2\sqrt{a\,(1-e^2)}\cos i = T \tag{38}$$

Now we assume that the spacecraft's orbit crosses the minor body orbit. At the crossing point, we can write the v_∞ as:

$$v_\infty^2 = 1 + v^2 - 2v\cos\gamma\cos i \tag{39}$$

where γ is the flight path angle. We recall the *vis-viva* equation for $r = 1$ and $\mu \to 0$ and the expression of the angular momentum

$$\frac{1}{a} = 2 - v^2 \quad , \quad h = v\cos\gamma \tag{40}$$

to find:

$$\frac{1}{a} = 2 - v_\infty^2 + 1 - 2h\cos i \tag{41}$$

substituting Eq. (41) into Eq. (38) we finally find:

$$J \approx T = 3 - v_\infty^2 \tag{42}$$